September 4, 2014

Abstract

1 Introduction

This study examins the contribution of transient sources to the astrohpysical neutrino flux meassured by IceCube (HESE flux). The special focus will be placed upon Gamma Ray Bursts (GRBs).

Contrary to most studies which use external GRB triggers from satelites like Swift and Fermi, this result is based on the opposite idea of using neutrinos to trigger follow-up observations with Swift and optical telescopes. The disadavantage of this approach is the additional background while the advantage is the 2π field of view (FoV) (northern sky only) and the indepence of any gamma-ray sensitivity of the satelites. Instead of using real meassured GRBs, a Toy Monte Carlo was written to simulate the neutrino flux from a GRB population up to a redshift of eight. The GRB population and luminosity function is mainly based on a model by Wanderman and Piran (section **??**). Other models are included to study the model dependency.

The neutrino signal will be studied on the level of the Optical- and X-Ray Follow Up - O(X)FU - and compared to the meassured data. The OFU is described in more detail in section **??**.

The GRB population model, simulated GRB neutrinos and experimental results will be combined within the analysis frame work of the GRB population Toy Monte Carlo. It is explained in more detail in section **??** while the main results are summarized and discussed in section **??**.

Differential co-moving shell volume	$dV = 4\pi D_H \frac{(1+z)^2 D_a^2(z)}{K(z)} dz$
Hubble distance	$D_H = \frac{c}{H_0} = 3000 h^{-1}\text{Mpc}$
angular distance	$D_a(z) = (1+z)^{-2} D_l(z)$
	$K(z) = \sqrt{\Omega_m (1+z)^3 + \Omega_\Lambda}$
Parameters	$h = 0.7$, $\Omega_m = 0.3$, Ω_Λ

Table 1: Cosmological definitions

2 GRB models

Most GRB analyises within IceCube use information from observed GRBs to look for neutrino clusters in time and space correlation with the detected GRBs. This strategy has the obvious advantague of reducing the neutrino background to achieve higher significance per GRB observation. However, due to the limited Field of View of the satelites there will be many GRBs that stay undetected. Furthermore, one is biased by the detection sensitivity of the satelites.

In this analysis, a GRB population is assumed based on theoretical work and extrapolation based on data from Swift and other satelites. The redshift and luminosity functions are extracted. The neutrino luminosity function is assumed to have the same shape and is shifted in energy by an efficiency factor ε (see section ???). The different population models under consideration are discussed in this chapter.

The main analysis has been done based on the luminosity function and GRB rate density calculated by Wanderman and Piran (**??**). The other models presented here were considered to examine the dependency on the assumed model.

2.1 Wanderman Piran

Wanderman and Piran (reference ???) extracted a GRB distribution in redshift and luminosity using GRB data up to 2011 (????) applying detection efficiencies for both the detection in γ- rays and a following determination of the host redshift.

The differential co-moving rate of bursts (fig. **??**) at a redhisft z is

$$R(z) = \frac{R_{\mathrm{GRB}}(z)}{(1+z)} \frac{dV(z)}{dz} \tag{2.1}$$

$dV(z)/dz$ is the differential co-moving shell volume (table **??**) and the factor $(1+z)^{-1}$ reflects the cosmological time dilation. R_{GRB} is fitted to data with the result (fig **??**)

$$R_{\mathrm{GRB}}(z) = \begin{cases} \rho_0 \cdot (1+z)^{n_1} & z \leq z_1 \\ \rho_0 \cdot (1+z_1)^{n_1-n_2} (1+z)^{n_2} & z > z_1 \end{cases} \tag{2.2}$$

with $n_1 = 2.07$, $n_2 = -1.36$, $z_1 = 3.11$ and the local rate $\rho_0 = 1.25 \mathrm{Gpc}^{-3}\mathrm{yr}^{-1}$.

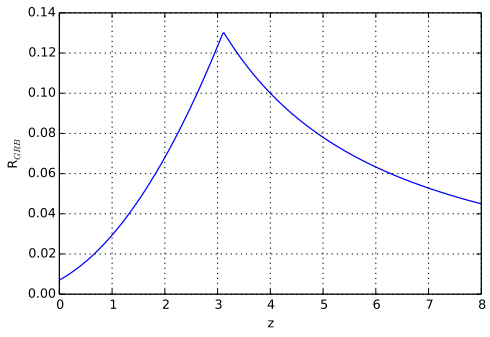

Figure 1

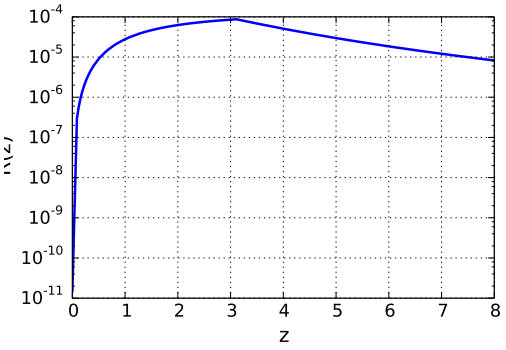

Figure 2: Differential co-moving rate

The peak γ-luminosity at the source L_{Peak} (fig. **??**) is determined to follow

$$L_{\mathrm{Peak}} = \begin{cases} \left(\frac{L}{L_*}\right)^{-\alpha} & L < L_* \\ \left(\frac{L}{L_*}\right)^{-\beta} & L > L_* \end{cases} \tag{2.3}$$

in which $\log_{10} L_* = 52.53$ erg / s is the break luminosity and $\alpha = 0.17$ and $\beta = 1.44$ are the spectral indices (table **??**). No redshift evolution is assumed.

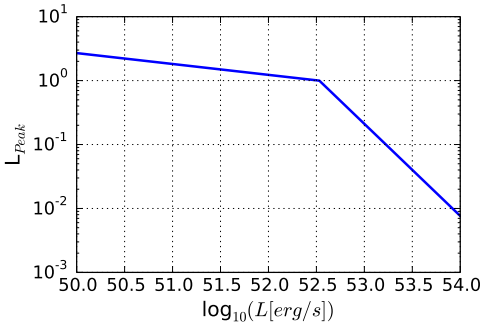

Figure 3

Model	$\log_{10}\left(L_*\left[\text{erg s}^{-1}\right]\right)$	α	β	$\rho_0\left[\text{Gpc}^{-3}\ \text{yr}^{-1}\right]$	z_1	n_1	n_2	N_{GRB}
WP	52.53	0.17	1.44	1.25	3.11	2.07	-1.36	9082.83
HC 1	51.9	0.95	2.59	0.48	3.6	2.1	-0.7	4791.97
HC 2	51.7	0.13	2.42	0.48	3.6	2.1	-0.7	4791.97

Table 2: Fit parameters to the luminosity functions and redshift distributions of the tested models.

2.2 Howell Coward

There is a more recent work (reference ???) by Howell, Coward, Stratta, Gendre and Zhou basing the redshift distribution on (rerference ???) and testing various luminosity functions. For purposes of readability it will be called Howell-Coward or HC-model.

Several luminosity functions were considered in (reference ???). Two of them will be compared to the model by Wanderman and Piran. They are designated HC1 and HC2.

Similarly to Wanderman and Piran, the luminosity is assumed to not evolve with redshift in their main work. The same function are used for redshift distribution (eq. **??**) and luminosity functions (eq. **??**) as in WP, but different fit results were obtained for the parameters (Table **??**).

The considered luminosity range is with $\log_{10}L_{\text{Peak}} \in (49,57)$ larger than in WP ($\log_{10}L_{\text{Peak}} \in (50,54)$). The break peak luminosity is in both HC models lower than in WP transitioning into a harder slope towards higher luminosities (Fig. **??**). At lower luminosities the slopes of HC2 and WP are quite similar (0.13, 0.17) while more low luminosity GRBs are expected in HC1.

The redshift distribution in HC is shifted to smaller values of $R(z)$ as a smaller local rate and total number of GRBs is assumed (Table **??**). The rise to the break redshift is quite similar to WP though the break is at higher redshifts (3.6 compared to 3.11) transitioning into a slower decay at large z. The overall impact are more distant GRBs in HC than in WP which should lead to a slight weakening of the limits.

While most of cases discussed in (reference ???) imply independentend luminosity and redshift, a correction is given to examine the influence of a possible evolution. This will be added at a later point as a third comparison model.

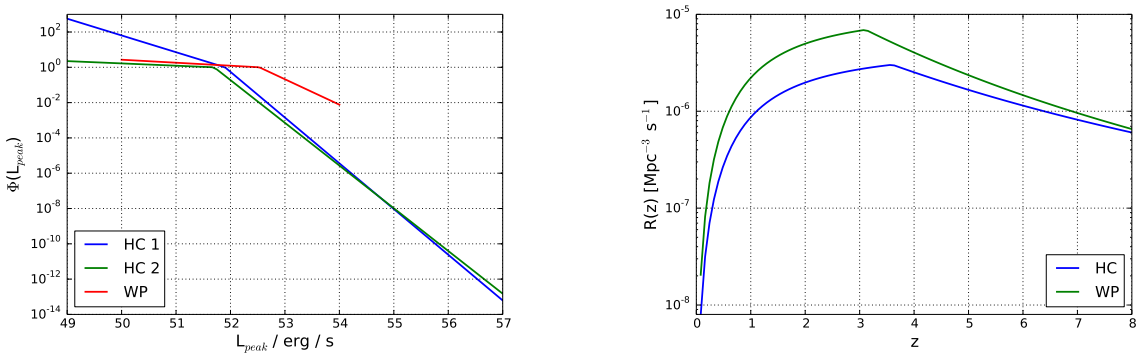

(a) Luminosity functions

(b) Redshift distributions

Figure 4: The luminosity functions (left) from the Wanderman-Piran model and two functions from the HC model on the left. The WP only take into account luminosities in the range of $10^{50} - 10^{54}$ erg / s which is reflected in the shorter red line.
The redshift distributions (right) develop similar up to $z = 3.11$ at which point it breaks for the WP-model. The HC predicts more GRBs at higher redshift values.

2.3 Long low luminosity GRBs

In recent years, IceCube has started to rule out the first optimistic GRB neutrino emission models leading to new ideas as to possible neutrino emitters. It has been proposed (reference ???) that a high number of very low luminosity GRBs exists that are difficult to detect in γ-rays but could produce most of the neutrinos expected from GRBs. In principle, the follow-up analysis based on IceCube triggers can be an approach to examine these objects. Thus they are discussed here briefly for completeness sake.

Unfortunately, these low luminosity GRBs are predicted to have a prompt emission phase in the range of 10^3 s. The follow-up program surpresses background by allowing a maximal time difference of 100s between two events reducing the sensitivity to very long GRBs at the same time. Therefore, they have not been examined yet within this analysis.

2.4 Supernovae

To be added

2.5 T90

Ninety percent of the detectable γ-ray flux is received between a time intervall called t_{90}. Reference (???) lists values for most GRBs. The extracted values for long GRBs are displayed in figure **??**.

In the GRB Toy Monte Carlo t_{90} values will be drawn at source (marked with$\hat{}$) to calculate the total energy output according to

$$P(\hat{t}_{90}) = a \cdot \exp\left(-\frac{(\hat{t}_{90} - b)^2}{2c^2}\right). \tag{2.4}$$

It will be folded with the drawn redshift to calculate the t_{90} pervieved at earth.

$$t_{90} = \hat{t}_{90} \cdot (1+z) \tag{2.5}$$

The t_{90} distributions for the WP and HC models are displayed in figure **??** as well.

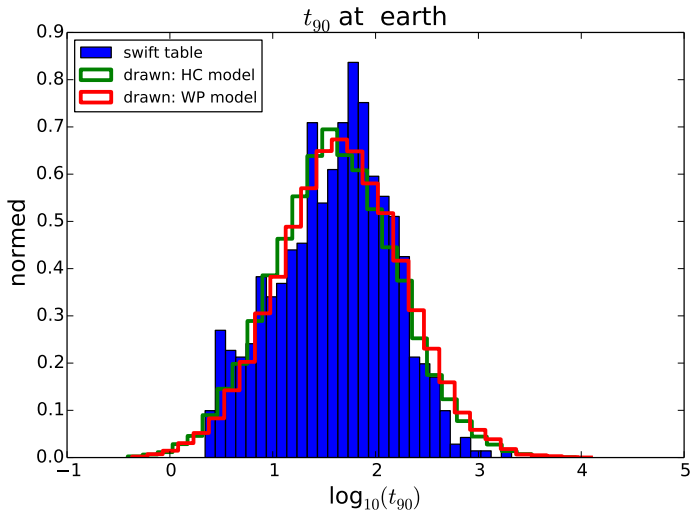

Figure 5: The t_{90} distributions at earth based on data extracted from the Swift database (reference ???) and the drawn distributions based on t_{90} values drawn at source and folded with the redshift distributions.

3 Optical- and X-Ray Follow Up

To be added

4 GRB Toy Monte Carlo

The previous chapters have laid the ground work on which the GRB Population Toy Monte Carlo is built. This chapter describes how GRBs are being drawn according to the models described in section ??? and how the neutrino signal expectation within IceCube is calculated.

What about GRB counting and so on?

test statistic? next chapter?

4.1 GRB Spectra

The astrophysical neutrinos discovered by IceCube can be described by various spectra depending on the data and conditions set for the fit. This analysis examines three different scenarios.

The first two scenarios are based on global fits not only to the HESE events but to other datasets as well. Once a fit with a cut-off was chosen and once the index of the power law was free. The third fit is exclusevly based on the HESE data with a free index:

Global fit: cut-off

$$E^2\Phi = 0.9 \cdot 10^{-8} \cdot \exp\left(-\frac{E}{2.8\ \text{PeV}}\right) \text{GeV s}^{-1}\ \text{sr}^{-1}\ \text{cm}^{-2} \tag{4.1}$$

Global fit: free index

$$E^2\Phi = 2.24 \cdot 10^{-8} \left(\frac{E}{100\ \text{PeV}}\right)^{-0.7} \cdot \exp\left(-\frac{E}{2.8\ \text{PeV}}\right) \text{GeV s}^{-1}\ \text{sr}^{-1}\ \text{cm}^{-2} \tag{4.2}$$

HESE fit: free index

$$E^2\Phi = 1.5 \cdot 10^{-8} \left(\frac{E}{100\ \text{PeV}}\right)^{-0.3} \cdot \exp\left(-\frac{E}{2.8\ \text{PeV}}\right) \text{GeV s}^{-1}\ \text{sr}^{-1}\ \text{cm}^{-2} \tag{4.3}$$

For the purpose of this analysis these spectra are assumed to be created by GRBs or other examined transient sources and as such a superposition of the individual GRB spectra. They are given the same shape. Generally, the flux follows the following formula which will be used in the following chapters for general calculations.

$$\Phi = \Phi_0 E^{-\gamma} \exp\left(-\frac{E}{\hat{E}_{cut}}\right) \tag{4.4}$$

The break energy $\hat{E}_{cut}$ is set to be a physics parameter that is the same for all GRBs. In case of scenario 1 it has to be optimized to reproduce the cutoff at earth of 2.8 PeV as good as possible. In the other two cases it is set to 10^{20} GeV and doesn't have any impact within the further analysis.

4.2 Drawing GRB properties

This section describes how properties such as the luminosity and the redshift are drawn according to their distribution ($f1$) specified in section **??**.

The function determines the maximum f_{max} and minimum f_{min} of $f1$ within a range in which a parameter p is to be drawn. The range is specified by the user.

In the next step it randomly throws a value $p1$ for p within the specified range and a random value f_{random} between f_{min} and f_{max}. Is $f_{random} <= f(p1)$ fullfilled, then p1 is returned as a value for p according to the distribution $f1$. Otherwise the step is repeated until the condition is met.

The following parameters are drawn:

- Peak luminosity L_{Peak}
- Redshift z
- Zenith angle θ (uniform in $\cos(\theta)$)

- Azimuth angle ϕ (uniform)
- $t_{90,S}$

4.3 Number of expected Neutrinos based on NuGen Datasets

The simulation uses nugen datasets to calculate the number of expected neutrinos according to the standard formula (cite ???).

$$N_{\text{exp}}^{\nu} = \sum_i \frac{dF_P(E_i)}{dE_i} \cdot \frac{OneWeight_i}{N_{\text{generated}}} \tag{4.5}$$

The nugen simulation describes the probability for each simulated neutrino event i to reach the detector, interact within its effective volume and to be detected ($OneWeight_i$), the individual energy E_i and the number of generated MC neutrino events $N_{\text{generated}}$.

The differential particle fluence $\frac{dF_P}{dE}$ at earth needs to be calculated based on the GRB properties drawn at source - peak luminosity $\hat{L}_{\text{Peak}}$, $\hat{t}_{90,S}$, redshift (sections **??** - **??**). They are marked with a hat.

4.3.1 Zenith Bands

The probability to detect a neutrino is highly dependent on the zenith angle of its origin. The number of expected neutrinos within IceCube can be calculated for all simulated events (eq. **??**). However, these are distributed over the whole sky and might not represent a GRB from a specific direction very well. Therefore only events from a zenith region around a drawn direction will be used to calculate the expected signal. The true direction of each considered event needs to be within a range around the GRB direction in CosΘ

$$\text{Cos}\,(\Theta_{\nu,\text{true}}) \in [\text{Cos}\,(\Theta_{\text{GRB}}) - ZBW, \text{Cos}\,(\Theta_{\text{GRB}}) + ZBW] \tag{4.6}$$

The zenith band width is set to $ZBW = 0.05$ and equal in cosinus of the zenith angle to achieve similar (and enough) statistics near pole and horizon.

Consequently, the number of expected neutrino events within the detector (eq. **??**) is not calculated anymore based on the total number of generated events $N_{\text{generated}}$ over the whole sky but only a fraction of events within the zenith band. Therefore, $N_{\text{generated}}$ needs to be replaced by an effective number of generated events

$$N_{\text{generated}}^{\text{eff}} = N_{\text{generated}} \cdot \frac{A_{ZB}}{4\pi} \tag{4.7}$$

in which A_{ZB} is the area of the zenith band. The number of expected neutrinos is then

$$N_{\text{exp}}^{\nu} = \sum_i \frac{dF_P(E_i)}{dE_i} \cdot \frac{OneWeight_i}{N_{\text{generated}}} \tag{4.8}$$

4.4 Shift Event Position to GRB position

In later steps the directions of different neutrino events will be compared to each other. Therefore, all events within a zenith band need to be shifted such that their true direction $\vec{t}$ will coincide with the GRB direction $\vec{g}$ and the shifted or new reconstructed direction $\vec{n}$ should have the same distance and direction to $\vec{g}$ as the originally reconstructed direction $\vec{r}$ had to $\vec{t}$.

The following calculations will be made in cartesian coordinates by transforming the zenith and azimuth angle

$$\begin{aligned} x &= \sin\theta \cdot \cos\phi \\ y &= \sin\theta \cdot \sin\phi \\ z &= \cos\theta \end{aligned} \tag{4.9}$$

with $\phi \in [0, 2\pi)$, $\theta \in [0, \pi]$ The angular difference between $\vec{t}$ and $\vec{r}$ is

$$\cos\alpha = \frac{\vec{r} \cdot \vec{t}}{|\vec{r}||\vec{t}|} \tag{4.10}$$

and the direction of $\vec{r}$ relative to $\vec{t}$ is

$$\vec{e} = \frac{\vec{r}-\vec{t}}{|\vec{r}-\vec{t}|} \tag{4.11}$$

Therefore, the following conditions need to be met

$$\cos\alpha = \frac{\vec{r}\cdot\vec{t}}{|\vec{r}||\vec{t}|} = \frac{\vec{n}\cdot\vec{g}}{|\vec{n}||\vec{g}|} \tag{4.12}$$

$$\vec{n} = \vec{g} + c\vec{e} \tag{4.13}$$

leaving the factor c to be the only unkown to determine $\vec{n}$. There should be two solutions, one in the positive and one in the negative direction yealding two possible vectors that fullfill the same angular distance to the GRB direction $\vec{g}$. As $\vec{e}$ points into the intended direction, c will be always chosen as positive.

Combining the conditions, one can derive the factor c

$$\begin{aligned}
\cos\alpha &= \frac{\vec{n}\cdot\vec{g}}{|\vec{n}||\vec{g}|} \\
&= \frac{(\vec{g}+c\vec{e})\cdot\vec{g}}{|\vec{g}+c\vec{e}||\vec{g}|} \\
&= \frac{(g_x + c\cdot e_x)\cdot g_x + (g_y + c\cdot e_y)\cdot g_y + (g_z + c\cdot e_z)\cdot g_z}{\sqrt{(g_x+ce_x)^2+(g_y+ce_y)^2+(g_z+ce_z)^2}\cdot\sqrt{g_x^2+g_y^2+g_z^2}} \\
&= \frac{g_x^2+g_y^2+g_z^2 + c\cdot(e_xg_x+e_yg_y+e_zg_z)}{\sqrt{g_x^2+g_y^2+g_z^2+2c\cdot(e_xg_x+e_yg_y+e_zg_z)+c^2\left(e_x^2+e_y^2+e_z^2\right)}\cdot\sqrt{g_x^2+g_y^2+g_z^2}} \\
&= \frac{\gamma + c\cdot\tau}{\sqrt{\gamma+2c\cdot\tau+c^2\cdot\zeta}\sqrt{\gamma}}
\end{aligned} \tag{4.14}$$

with the abbreviations

$$\begin{aligned}
\gamma &= \vec{g}^2 = g_x^2+g_y^2+g_z^2 \\
\tau &= \vec{g}\cdot\vec{e} = e_xg_x+e_yg_y+e_zg_z \\
\zeta &= \vec{e}^2 = e_x^2+e_y^2+e_z^2
\end{aligned} \tag{4.15}$$

Calculating the square of equation **??** and rewriting it to fit the standard p,q - formulism, one obtains

$$\begin{aligned}
\left(\gamma+2c\cdot\tau+c^2\cdot\zeta\right)\gamma\cdot\cos^2\alpha - \left(\gamma^2+2c\tau\gamma+c^2\tau^2\right) &= 0 \\
\cos^2\alpha\left(\gamma^2+2c\cdot\tau\gamma+c^2\cdot\zeta\gamma\right) - \left(\gamma^2+2c\tau\gamma+c^2\tau^2\right) &= 0 \\
c^2\cdot\left(\zeta\gamma\cos^2\alpha-\tau^2\right) + 2c\cdot\tau\gamma\left(\cos^2\alpha-1\right) + \gamma^2\left(\cos^2\alpha-1\right) &= 0 \\
c^2 + c\cdot\frac{2\tau\gamma\left(\cos^2\alpha-1\right)}{\zeta\gamma\cos^2\alpha-\tau^2} + \frac{\gamma^2\left(\cos^2\alpha-1\right)}{\zeta\gamma\cos^2\alpha-\tau^2} &= 0 \\
c^2 + p\cdot c + q &= 0
\end{aligned} \tag{4.16}$$

Therefore, c has two solutions as predicted. The positive will always be chosen.

$$c = -\frac{\tau\gamma\left(\cos^2\alpha-1\right)}{\zeta\gamma\cos^2\alpha-\tau^2} \pm \sqrt{\left(\frac{\tau\gamma(\cos^2\alpha-1)}{\zeta\gamma\cos^2\alpha-\tau^2}\right)^2 - \frac{\gamma^2\left(\cos^2\alpha-1\right)}{\zeta\gamma\cos^2\alpha-\tau^2}} \tag{4.17}$$

The value of c leads to the calculation of the new reconstructed direction $\vec{n}$ which can be transformed back into spherical coordinates using

$$\theta = \arccos\left(\frac{n_z}{|\vec{n}|}\right) \tag{4.18}$$

$$\begin{aligned}
\phi &= \arctan\left(\frac{n_y}{n_x}\right), \text{ if } n_x > 0 \\
\phi &= sign\,(n_y)\cdot\frac{\pi}{2}, \text{ if } n_x = 0 \\
\phi &= \arctan\left(\frac{n_y}{n_x}\right) + \pi, \text{ if } n_x < 0 \text{ and } n_y \geq 0 \\
\phi &= \arctan\left(\frac{n_y}{n_x}\right) - \pi, \text{ else}
\end{aligned} \tag{4.19}$$

Figure **??** demonstrates that the new directions are for almost all events at the same distance to the GRB as the originally reconstructed directions are compared to their true directions.

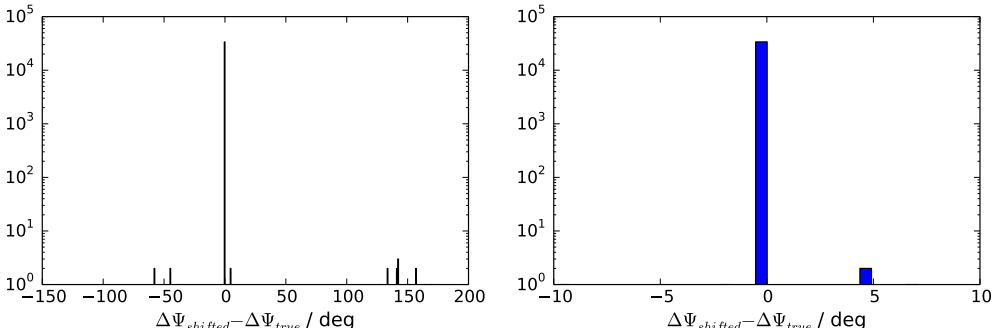

Figure 6: Shown is the difference between the true error between reconstructed and true direction and the error between the shifted reconstructed direction and the GRB direction. The left plot includes all events while the right one zooms in to a small range.

4.4.1 Total Emitted Energy as Source $\hat{E}_{\nu,\text{total}}$

So far, the steps dealing with simulation effects and neutrino directions have been described. To calculate N_{exp}^{ν} the differential particle fluence in energy at earth needs to be calculated as well, based on parameters that are drawn as part of the simluation (chapter **??**). A first step is to calculate the total emitted energy in neutrino at the source $\hat{E}_{\nu,\text{total}}$.

The peak luminosity and the 90% time window can be used if the light curve is known. In this work a fast rise and rapid decay (FRED) light curve with an instant jump to the peak luminosity and an exponential decay afterwards is assumed.

The luminosity at a given time is defined as

$$\hat{L}(\hat{t}) = \hat{L}_{\text{Peak}} \cdot e^{\left(-\frac{\hat{t}}{\hat{\tau}}\right)} \tag{4.20}$$

The total energy is the time integral over the time dependent luminosity distribution

$$\begin{aligned} \hat{E}_{\nu,\text{total}} &= \int_0^{\infty} \hat{L}(\hat{t})d\hat{t} = L_{\text{Peak}} \int_0^{\infty} e^{-\frac{t}{\hat{\tau}}} dt \\ &= -\hat{\tau} \cdot \hat{L}_{\text{Peak}} \left[e^{-\frac{\hat{t}}{\hat{\tau}}}\right]_0^{\infty} = \hat{\tau} \cdot \hat{L}_{\text{Peak}} \end{aligned} \tag{4.21}$$

The final shape of the distribution depends on the unknown τ which needs to be replaced by a known quantity such as the 90 % time window $\hat{t}_{90}$ in which 90% or $\hat{E}_{\nu,90} = 0.9 \cdot \hat{E}_{\nu,\text{total}}$ were observed. The amount of energy radiated within this time can be determined with

$$\begin{aligned} \hat{E}_{\nu,90} = 0.9 \cdot \hat{E}_{\nu,\text{total}} = 0.9 \cdot \hat{\tau}\hat{L}_{\text{Peak}} &= \int_0^{\hat{t}_{90}} \hat{L}(\hat{t})d\hat{t} \\ = -\hat{\tau}\hat{L}_{\text{Peak}} \left[e^{-\frac{\hat{t}}{\hat{\tau}}}\right]_0^{\hat{t}_{90}} &= \hat{\tau}\hat{L}_{\text{Peak}} \left[1 - e^{-\frac{\hat{t}_{90}}{\hat{\tau}}}\right] \end{aligned} \tag{4.22}$$

leading to

$$\begin{aligned} \left[1 - e^{-\frac{\hat{t}_{90}}{\hat{\tau}}}\right] &= 0.9 \\ 0.1 &= e^{-\frac{\hat{t}_{90}}{\hat{\tau}}} \\ \ln(0.1) &= -\frac{\hat{t}_{90}}{\hat{\tau}} \\ \Rightarrow \hat{\tau} &= \frac{-\hat{t}_{90}}{\ln(0.1)} \end{aligned} \tag{4.23}$$

Entering this in equation **??** leads to:

$$\hat{E}_{\nu,\text{total}} = -\hat{L}_{\text{Peak}} \frac{\hat{t}_{90}}{\ln(0.1)} \tag{4.24}$$

4.4.2 Fluence at Source

The simulation draws GRB properties at source. In the first step they are used to calculate the differential particle fluence in energy $\frac{d\hat{F}_P}{d\hat{E}}$ in units $\mathrm{GeV}^{-1}\mathrm{s}^{-1}\mathrm{sr}^{-1}\mathrm{cm}^{-2}$ at a small co-moving distance from the source $\hat{d}_0$. The spectral shape is a generalization based on the fits to the HESE flux (eq. **??**).

$$\frac{d\hat{F}_P}{d\hat{E}} = \frac{\hat{F}_0}{4\pi\hat{d}_0^2} \cdot \hat{E}^{-\gamma} \exp\left(-\frac{\hat{E}}{\hat{E}_{\mathrm{cut}}}\right) \tag{4.25}$$

The fluence normalization $\hat{F}_0$ is unknown. However, in the previous section **??** the total emitted energy was calculated. It equals the integral over $\hat{E} \cdot \frac{d\hat{F}_P}{d\hat{E}}$.

$$\hat{E}_{\nu,\mathrm{total}} = \int_{\hat{E}_{min}}^{\infty} \hat{E}\hat{F}_0\hat{E}^{-\gamma} \exp\left(-\frac{\hat{E}}{\hat{E}_{\mathrm{cut}}}\right) d\hat{E} = \hat{F}_0 \Upsilon\left(\hat{E}_{min}, \hat{E}_{\mathrm{cut}}\right) \tag{4.26}$$

The result depends on two GRB parameters which are chosen equally in for all GRBs: A minimal energy of the neutrinos $\hat{E}_{min}$ and the break energy $\hat{E}_{cut}$. Once, these parameters are chosen, Υ is a constant for all GRBs and the differential particle fluence in energy at source can be written as

$$\frac{d\hat{F}_P}{d\hat{E}} = \frac{\hat{E}_{\nu,\mathrm{total}}}{4\pi d_0^2 \Upsilon\left(\hat{E}_{min}, \hat{E}_{\mathrm{cut}}\right)} \cdot \hat{E}^{-\gamma} \exp\left(-\frac{\hat{E}}{\hat{E}_{\mathrm{cut}}}\right) \tag{4.27}$$

4.4.3 Fluence at Earth

Having derived the fluence at source, cosmological effects need to be taken into account when calculating the fluence at earth. The energy and time at source relate to the values at earth with $\hat{E} = (1+z)E$ and $\hat{t} = \frac{t}{1+z}$. The energy flux at earth Φ_E is linked to the luminosity via

$$\Phi_E(t) = \frac{\hat{L}\left(\hat{E}, \hat{t}\right)}{4\pi d_l^2} = \frac{L(E,t)}{4\pi d_l^2} \tag{4.28}$$

with the luminosity distance $d_l = (1+z) \cdot d_c$. The particle fluence F_P at earth is the time integrated particle flux Φ_P which in turn is the energy derivative of the energy flux.

$$F_P(E) = \int \Phi_P(E,t)\, dt = \int \frac{d\Phi_E(E,t)}{dE}\, dt \tag{4.29}$$

The energy flux can be replaced with the luminosity according to **??**. Applying a derivation in energy and transforming energy and time to the source frame, one obtains

$$\begin{aligned} \frac{dF_P(E)}{dE} &= \frac{1}{4\pi d_l^2} \int \frac{d^2L(t)}{dE^2} dt & (4.30)\\ &= \frac{1}{4\pi d_l^2} \int \frac{d^2L(\hat{t})}{d\hat{E}^2} \frac{d^2\hat{E}}{dE^2} \frac{dt}{d\hat{t}} d\hat{t} & (4.31)\\ &= \frac{(1+z)^3}{4\pi d_l^2} \int \frac{d^2L(\hat{t})}{d\hat{E}^2} d\hat{t} & (4.32) \end{aligned}$$

A similar equation is true for differential particle fluence in energy near the source at a distance d_0.

$$\frac{d\hat{F}_P(\hat{E})}{d\hat{E}} = \frac{1}{4\pi d_0^2} \int \frac{d^2L(\hat{t})}{d\hat{E}^2} d\hat{t} \tag{4.33}$$

Combining equation **??** and **??** relates the differential particle fluence at earth to the differential particle fluence at

source derived in **??**.

$$\frac{dF_P(E)}{dE} = \left(\frac{d_0}{d_l}\right)^2 (1+z)^3 \frac{d\hat{F}_P(\hat{E})}{d\hat{E}} \tag{4.34}$$

$$= \frac{\hat{E}_{\nu,\text{total}}}{4\pi d_l^2 \Upsilon\left(\hat{E}_{min}, \hat{E}_{\text{cut}}\right)} \cdot \hat{E}^{-\gamma} \exp\left(-\frac{\hat{E}}{\hat{E}_{\text{cut}}}\right) \cdot (1+z)^3 \tag{4.35}$$

$$= \frac{\hat{E}_{\nu,\text{total}}}{4\pi d_l^2 \Upsilon\left(\hat{E}_{min}, \hat{E}_{\text{cut}}\right)} \cdot E^{-\gamma} \exp\left(-\frac{E \cdot (1+z)}{\hat{E}_{\text{cut}}}\right) \cdot (1+z)^{3-\gamma} \tag{4.36}$$

In the last step the energy at source was replaced with the energy at earth in consideration of the cosmological effects. This formula can now be used to calculate the number of expected neutrinos within IceCube given the drawn properties and a nugen dataset (section **??**).

4.4.4 Number of Expected Neutrinos Within IceCube

This chapter described how the differential particle fluence in energy can be derived from the drawn parameters describing a GRB in this simulation. The number of expected neutrinos is given with

$$\begin{aligned} N_{\text{exp}}^{\nu} &= \sum_i \frac{dF_P(E_i)}{dE} \cdot \frac{OneWeight_i}{N_{\text{generated}} \cdot A_{ZB}} \\ &= \sum_i \cdot \frac{\hat{E}_{\nu,\text{total}}}{4\pi d_l^2 \Upsilon\left(\hat{E}_{min}, \hat{E}_{\text{cut}}\right)} \cdot E_i^{-\gamma} \exp\left(-\frac{E_i \cdot (1+z)}{\hat{E}_{\text{cut}}}\right) \cdot (1+z)^{3-\gamma} \frac{OneWeight_i}{N_{\text{generated}} \cdot \frac{A_{ZB}}{4\pi}} \end{aligned} \tag{4.37}$$

It is dependent on various factors of the nugen simulation and some parameters from the derivation of the differential particle fluence. The nugen simulation describes the probability for each simulated event i to reach the detector, interact within its effective volume and to be detected ($OneWeight_i$), the individual energy E_i, the number of generated MC neutrino events $N_{\text{generated}}$ and a re-weighting factor $\frac{A_{ZB}}{4\pi}$. The re-weighting factor will be explained in more detail in section ???.

Furthermore, the number of expected neutrino is dependent on the redshift of the GRB, the total emitted energy in neutrinos $\hat{E}_{\nu,\text{total}}$ - and thus $\hat{L}_{\text{Peak}}$ and $\hat{t}_{90}$ - as well as the constant Υ. The constant itself is dependent on the energy of the cut-off $\hat{E}_{\text{cut}}$ and the minimal neutrino energy at source $\hat{E}_{min}$. As described in ??? the cut-off energy will be optimized to reproduce the observed cut-off or set to very high values depending on the spectrum that is used (see ???). The effect of the minimal energy can be either absorbed into the normalization to the HESE flux (chapter **??**) or specific cases and their impact can be studied (chapter ???).

4.5 Normalization to HESE Flux

The luminosity is drawn according to the luminosity function fitted to gamma-ray data, assuming the neutrino luminosity function to follow the same shape. However, a normalization factor might be needed to trim it to the correct energies and consequently to the correct number of neutrinos to produce the HESE flux. ($N_{\text{exp}}^{\nu} \propto \hat{E}_{\nu,\text{total}} \propto L_{\text{Peak}}$). Equation **??** evolves to

$$N_{\text{exp}}^{\nu} = \varepsilon \cdot \sum_i \cdot \frac{\hat{E}_{\nu,\text{total}}}{4\pi d_l^2 \Upsilon\left(\hat{E}_{min}, \hat{E}_{\text{cut}}\right)} \cdot E_i^{-\gamma} \exp\left(-\frac{E_i \cdot (1+z)}{\hat{E}_{\text{cut}}}\right) \cdot (1+z)^{3-\gamma} \frac{OneWeight_i}{N_{\text{generated}} \cdot \frac{A_{ZB}}{4\pi}} \tag{4.38}$$

$$= \varepsilon^* \cdot \sum_i \cdot \frac{\hat{E}_{\nu,\text{total}}}{4\pi d_l^2} \cdot E_i^{-\gamma} \exp\left(-\frac{E_i \cdot (1+z)}{\hat{E}_{\text{cut}}}\right) \cdot (1+z)^{3-\gamma} \frac{OneWeight_i}{N_{\text{generated}} \cdot \frac{A_{ZB}}{4\pi}} \tag{4.39}$$

Once $\hat{E}_{min}$ (chapter ???) and $\hat{E}_{\text{cut}}$ are determined, Υ is a constant for every GRB which can be included in an effective normalization factor

$$\varepsilon^* = \frac{\varepsilon}{\Upsilon\left(\hat{E}_{min}, \hat{E}_{\text{cut}}\right)} \tag{4.40}$$

Due to the effective normalization factor it is redundant to calculate the constant Υ. However, a different ε^* needs to be determined for different $\hat{E}_{min}$. The impact of choosing different minimal energies is studied in chapter ???.

There are two ways to determine ε - a Monte Carlo based and a semi analytic one.

4.5.1 ε^* - Monte Carlo Based

This approach was followed by Nora Strotjohann. Given the different spectra fitted to the HESE flux (chapter **??**), a different number of neutrinos per year are expected due to GRBs. Using the nugen simulation without the GRB simulation one can simply calculate the number of neutrinos using the spectra fitted at earth. They are displayed in figure **??**. Their shape is quite similar at high energies at which the HESE events were found. However, the curves diverge quite significantly at lower energies leading to different predictions about the number of neutrinos one could expect from GRBs on OFU level.

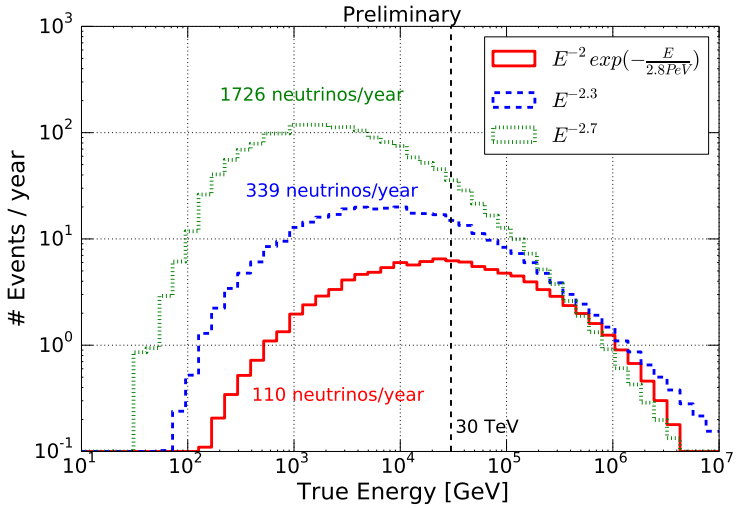

Figure 7: The three different spectra fitted to the HESE events on OFU level. The true neutrino energy is used. The number of expected neutrinos is highly dependent on the chosen spectrum.

To determine ε^* up to 5 million GRBs ($N_{\text{GRB, sim}}$) are simulated with ε^* set to one. The sum over N^{ν}_{exp} of all GRBs is renormalized to the number of expected GRBs per year $N_{\text{GRB, yr}}$ and needs to reproduce the number of expected neutrinos on OFU level.

$$\varepsilon^* = \frac{N^{\nu}_{\text{exp}}(\varepsilon^* = 1) \cdot \frac{N_{\text{GRB, yr}}}{N_{\text{GRB, sim}}}}{N^{\nu}_{\text{exp, OFU}}} \tag{4.41}$$

The final result depends on the number of expected GRBs per year which is an uncertain number. Fortunately, it is a linear factor and ε^* can be changed easily with the knowledge with which $N_{\text{GRB, yr}}$ it was calculated.

$$\varepsilon^*_{\text{new}} = \varepsilon^* \cdot \frac{N^{\text{new}}_{\text{GRB, yr}}}{N_{\text{GRB,yr}}} \tag{4.42}$$

4.5.2 ε^* - Semi-Analytic Approach

The second approach integrates over the expected differential fluxes in energy from all GRBs up to the maximal chosen redshift ($z_{max} = 8$) under consideration of their redshift distribution.

$$\Phi_{\text{GRB}} = \int_{z=0}^{z=8} dz R(z) \cdot \frac{dF_P\left(z, E, \hat{E}_{\nu,\text{total}}\left(\hat{t}_{90}, L_{\text{Peak}}\right)\right)}{dE} \tag{4.43}$$

$$= \int_{z=0}^{z=8} dz R(z) \cdot \frac{\hat{E}_{\nu,\text{total}}}{4\pi d_l^2(z)} \cdot E_i^{-\gamma} \exp\left(-\frac{E_i \cdot (1+z)}{\hat{E}_{\text{cut}}}\right) \cdot (1+z)^{3-\gamma} \tag{4.44}$$

The final result needs to equal the measured fluxes on earth over the whole energy range and the flux is recalculated for 100 energy values between 10 and 10^9 GeV evenly spaced in log$E$.

Next to the redshift of the GRBs and the energy of the neutrinos the signal expectation is dependent on the total energy in neutrinos and thus the peak luminosity and the $\hat{t}_{90}$ values. The average value is calculated based on an

average time window and peak luminosity. The average time window $< \hat{t}_{90} >$ was determined out of 5 million drawn values while the average peak luminosity is calculated according to

$$\begin{aligned} < L_{\text{Peak}} > &= \frac{\int_{L_{\text{Peak}}^{min}}^{L_{\text{Peak}}^{max}} L_{\text{Peak}} \cdot \Phi(L_{\text{Peak}}) d\log_{10} L_{\text{Peak}}}{\int_{L_{\text{Peak}}^{min}}^{L_{\text{Peak}}^{max}} \Phi(L_{\text{Peak}}) d\log_{10} L_{\text{Peak}}} \\ &= \frac{\int_{L_{\text{Peak}}^{min}}^{L_{\text{Peak}}^{max}} L_{\text{Peak}} \cdot \frac{\Phi(L_{\text{Peak}})}{L_{\text{Peak}} \ln(10)} dL_{\text{Peak}}}{\int_{L_{\text{Peak}}^{min}}^{L_{\text{Peak}}^{max}} \frac{\Phi(L_{\text{Peak}})}{L_{\text{Peak}} \ln(10)} dL_{\text{Peak}}} \\ &= \frac{\int_{L_{\text{Peak}}^{min}}^{L_{\text{Peak}}^{max}} \frac{\Phi(L_{\text{Peak}})}{\ln(10)} dL_{\text{Peak}}}{\int_{L_{\text{Peak}}^{min}}^{L_{\text{Peak}}^{max}} \frac{\Phi(L_{\text{Peak}})}{L_{\text{Peak}} \ln(10)} dL_{\text{Peak}}} \end{aligned} \tag{4.45}$$

The co-moving rate density $R(z)$ includes a normalization to the number of expected GRBs according to said model. If a different number of GRBs is assumed, then the resulting flux needs to be adjusted by an according factor.

This flux of all GRBs up to a redshift of eight needs to reproduce the HESE flux over the whole energy range (Fig. **??**). This can be achieved for the two spectra without a cut-off. However, the HESE flux can not be reproduced at very high energies using the same exponential cut-off for all GRBs at all redshifts. $\hat{E}_{\text{cut}}$ was chosen such that an exact agreement was reached for the most part of the energy range accepting a disagreement in the tail. Possibly, one could determine an energy dependent ε^*. However, given the few numbers of events at these energies and the lack of knowledge of the exact shape of the cut-off due to missing HESE statistic this extra complication was not attempted.

$$\varepsilon^* = \frac{\Phi_{\text{HESE}}(E)}{\Phi_{\text{GRB}}(E)} \tag{4.46}$$

The effective efficiency factor can be applied in the further simulation to each GRB using equation **??**.

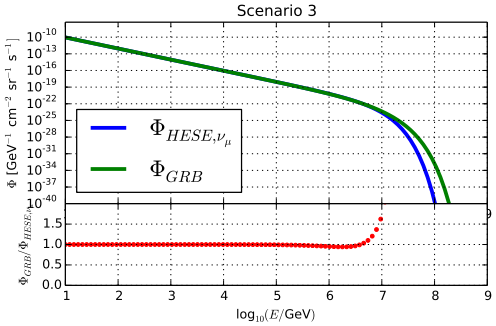

Figure 8: Upper plot: The differential flux in energy for the HESE spectrum (E^{-2} with cut-off) and the spectrum produced by all GRBs up to a redshift of 8.
Lower plot: ratio between the GRB flux and the HESE flux. The ratio should be queal to one.

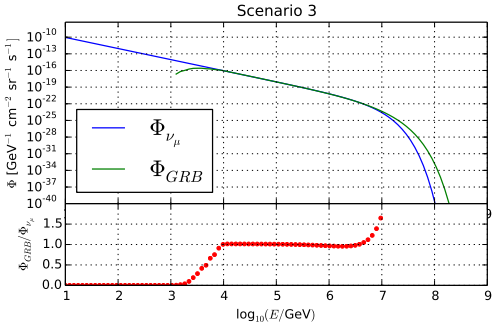

Figure 9: Upper plot: The differential flux in energy for the HESE spectrum (E^{-2} with cut-off) and the spectrum produced by all GRBs up to a redshift of 8. $\hat{E}_{min}$ was set to 10 TeV.
Lower plot: ratio between the GRB flux and the HESE flux. The ratio should be queal to one.

4.5.3 Influence of $\hat{E}_{min}$

The influence of the minimal neutrino energy from a GRB has two effects.

The constant Υ in eq. **??** becomes smaller the more stringent the energy cut is (Eq. **??**) leading to a smaller efficiency factor ε as the flux at each energy needs to reproduce the HESE flux. The effective efficiency factor ε^* will stay the same. Using the example of $\hat{E}_{min} = 10$ TeV shown in figure **??**, ε^* was chosen such that an agreement was found for as large an energy range as possible. Considering all energies (Fig. **??**) $\varepsilon^* = 0.149$ was determined

while applying a minimal energy leads to $\varepsilon^* = 0.151$. The discrepancy of about 1.5 % is probably due to the precision of agreement between the two fluxes required in the procedure.

The other effect can be seen at low energies at which the GRB flux drops to zero. No events with energies

$$E_\nu \leq \frac{\hat{E}_{min}}{1+z} \tag{4.47}$$

can exist in the detector if a minimal neutrino energy cut at source is applied. The GRB flux transitions from an agreement with the HESE flux towards no flux at all because the cut effects are redshift dependent and effect higher energies the closer to earth a GRB is assumed to be.

In summary, the effect of a different $\hat{E}_{min}$ on the final flux per energy is non existent. However, events will be lost at lower energies.

4.6 Detection Probabilities

At this stage, the drawing of GRB properties according to specified functions and the subsequent derivation and calculation of the signal expectation in IceCube has been explained. However, the Optical (and X-ray) Follow-Up does not trigger on singlets but on multiplets fulfilling several criteria.

Multiplets are a number of neutrinos that arrive within 100 s and 3.5 degrees of each other (chapter ???). A test statistic was implemented to select the most signal like doublets (chapter ???) to trigger Swift. Once triggered there is a chance that a source will not be within the FoV of the XRT.

4.6.1 Doublet Probabilities

4.6.1.1 $\mathbf{P}_{\Delta t}$

$P_{\Delta t}$ is the probability that two neutrinos arrive within 100 seconds, the time window specified in the doublet search. It falls exponentially with time if the lightcurve is assumed to be fast rising with an exponential decay (FRED)

$$P(\Delta t) = 1 - e^{\left(-\frac{\Delta t}{\tau}\right)} \tag{4.48}$$

in which τ can be determined according to equation **??** given the t_{90} drawn according to **??** and converted in agreement with **??**. For the Optical Follow-Up $\Delta t_{max} = 100$ s is currently set.

The effects of different time windows could be examined by choosing different values. However, this is not the focus of this work.

4.6.1.2 $\mathbf{P}_{3.5^\circ}$

The second requirement for each neutrino pair is that they arrive with a maximum angular separation of 3.5 degrees. To calculate the probability $P_{3.5^\circ}$ of this happening for a given GRB, nugen events need to be selected from within the zenith band (chapter **??**) and shifted to the GRB direction (chapter **??**). Each remaining event is paired with all other events, and the angular differences of the shifted reconstructed directions are determined. The probability is then the ratio between the sum of the weight products (eq. **??**) of all event pairs passing the 3.5° cut and all pairs

$$P_{3.5^\circ} = \frac{\sum_i \sum_{j=i+1} w_i \cdot w_j | \Delta\Psi(i,j) \leq 3.5^\circ}{\sum_i \sum_{j=i+1} w_i \cdot w_j} \tag{4.49}$$

This procedure takes a lot of computational power. However it is the same for all GRBs coming from the exact same zenith angle as the same nugen events will be considered.

Therefore, about ten thousand GRBs are drawn for each OFU cut setting and HESE spectra, the probability calculated and the result is used to parametrize the probability as a function of the GRB's zenith angle $P_{3.5^\circ}(\theta_{\mathrm{GRB}})$. The parameterization is then used to simulate GRBs in greater numbers.

4.6.1.3 $\mathbf{P}_{\mathbf{Doublet}}$

The probability that two neutrinos form a doublet that triggers OFU is then

$$P_{\mathrm{Doublet}} = P_{\Delta t} \cdot P_{3.5^\circ} \tag{4.50}$$

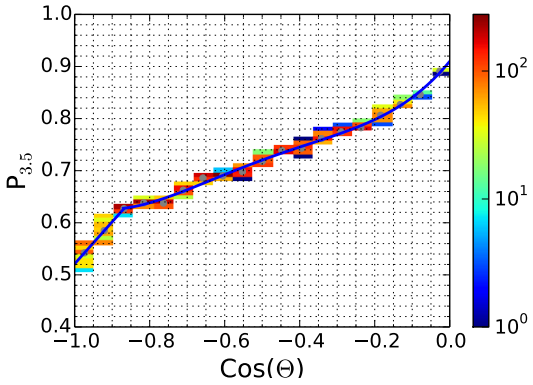

Figure 10: The probability of neutrino events to be within 3.5 % of each other and the dependency on the cosinus of the GRB zenith angle. The blue line represents the parameterization.

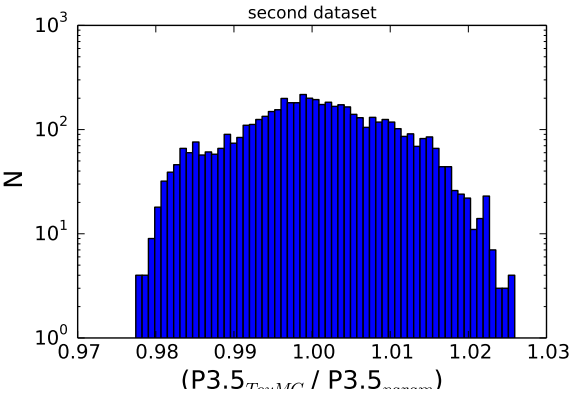

Figure 11: Using a second dataset, a histogram of the ratio between the calculated and parametrized values is shown. The maximum deviation is of about 2.5%.

4.6.1.4 P_{llh}

On average the doublet selection based on time and direction leads to about 50 - 60 doublets per year (depending on season) while only nine alerts can be sent to the Swift telescope. The selection of the most signal like doublets is based on the test statistic (chapter ???)

$$\begin{aligned}\lambda = -2\ln\mathscr{L} = \frac{\Delta\Psi^2}{\sigma_q^2} + 2\ln(2\pi\sigma_q^2) \\ - 2\ln\left(1 - e^{\frac{-\theta_A^2}{2\sigma_w^2}}\right) + 2\ln\left(\frac{\Delta T}{100\,\text{s}}\right)\end{aligned} \tag{4.51}$$

where the time between the neutrinos in the multiplet is denoted as ΔT and their angular separation as $\Delta\Psi$. $\sigma_q^2 = \sigma_1^2 + \sigma_2^2$ and $\sigma_w^2 = \left(1/\sigma_1^2 + 1/\sigma_2^2\right)^{-1}$ with σ_1 and σ_2 are the uncertainties on the directional reconstruction of the two neutrino events. θ_A corresponds to the (circularized) angular radius of the field of view (FoV) of the follow-up telescope (set to 0.5° for Swift). This test statistic is calculated for all event pairs that pass the condition of being reconstructed within 3.5°. The time difference is randomly drawn with $\Delta T \in [0, 100]$ s and weighted according to an exponential decay (Eq. **??**) introducing a dependency on t_{90} (Eq. **??**).

The Toy Monte Carlo requires a cut value λ_{cut} on the test statistic as input. The probability that a GRB doublet will pass the cut is determined by taking the ratio of the sum of weight products from events passing the cut and the sum of all doublets passed to this function.

$$P_{\text{llh}} = \frac{\sum_i \sum_{j=i+1} w_i \cdot w_j \mid \lambda(i,j) \leq \lambda_{\text{cut}} \mid \Delta\Psi(i,j) \leq 3.5^\circ}{\sum_i \sum_{j=i+1} w_i \cdot w_j \mid \Delta\Psi(i,j) \leq 3.5^\circ} \tag{4.52}$$

The parameterization of P_{llh} is more complicated than $P_{3.5^\circ}$. The test statistic depends not only on properties of simulated neutrino events and thus the zenith angle but on the time window between two neutrinos and thus t_{90}. Therefore, the data is split into ??? cosinus bin and the probability is fitted against the logarithm of the drawn t_{90} (Eq. **??** and **??**) value. An example is shown in figure **??**. The quality of the parameterization for all cosinus bins is tested using a second dataset and forming a histogram of the ratio between the simulated probability and the parametrized one. Most events are within 5% derivation however some differ up to 12%. The outlier's effects should average out by simulating a great number of GRBs (usually 5 million per dataset).

4.6.1.5 P_{onS}

The Optical Follow-Up program calculates the weighted mean direction from both events using the Cramer Rao error as weights. For a source to be detectable with Swift this direction must be within 0.5 degrees of the true source direction. The probability P_{onS} for two events to point back to the source well enough is given by the ratio of the sum over the event weight products fulfilling the condition and the sum over all event weight products:

$$P_{\text{onS}} = \frac{\sum_i \sum_{j=i+1} w_i \cdot w_j \mid \Psi_{\text{weighted mean}}(i,j) - \Psi_{GRB} \leq 0.5^\circ \mid \lambda(i,j) \leq \lambda_{\text{cut}} \mid \Delta\Psi(i,j) \leq 3.5^\circ}{\sum_i \sum_{j=i+1} w_i \cdot w_j \mid \lambda(i,j) \leq \lambda_{\text{cut}} \mid \Delta\Psi(i,j) \leq 3.5^\circ} \tag{4.53}$$

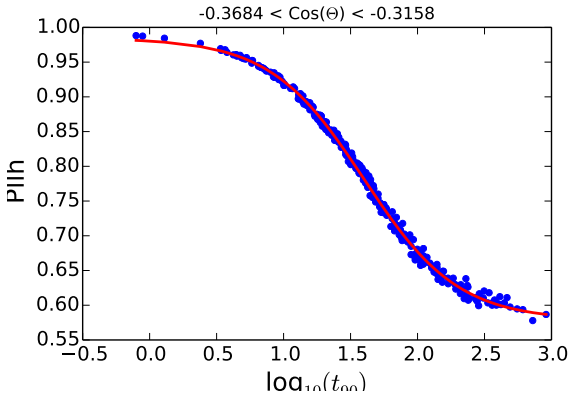

Figure 12: The probability of neutrino events to pass the cut on the test statistic and the dependency on the logarithm of the t_{90} value for a certain cosinus bin. The red line represents the parameterization.

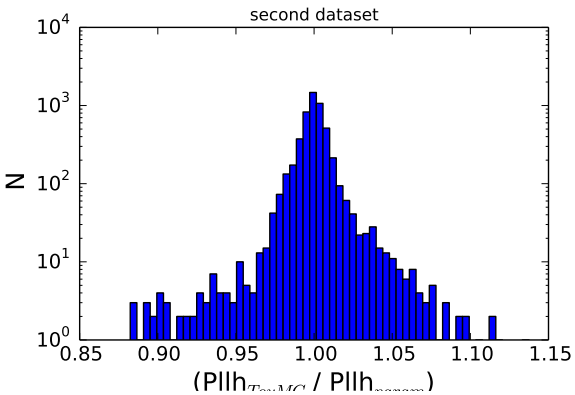

Figure 13: Using a second dataset, a histogram of the ratio between the calculated and parametrized values is shown. Most GRBs fall within 5% derivation while some outliers differ up to 12%.

It is parametrized with the same methods as P_{llh}.

4.6.2 Probability to Detect a GRB

In the previous sections the probabilities to have an XFU trigger were explained. They are calculated assuming the existence of two detected neutrinos. However, the number of expected neutrinos within IceCube (Eq. **??**) can be smaller or larger. The final probability to detect a GRB with the Optical Follow-Up considers the number of possible doublets - and thus possible higher multiplets. These considerations are described in this chapter.

5 Results

6 Discussion